Dark energy records in lensed cosmic microwave background

Viviana Acquaviva[1,2], Carlo Baccigalupi[1,2,3]
[1] *SISSA/ISAS, Astrophysics Sector, Via Beirut, 4, I-34014 Trieste, Italy*
[2] *INFN, Sezione di Trieste, Via Valerio 2, I-34014 Trieste, Italy*
[3] *Institut für Theoretische Astrophysik, Universität Heidelberg, Albert-Überle-Strasse 2, D-69120 Heidelberg, Germany*

We consider the weak lensing effect induced by linear cosmological perturbations on the cosmic microwave background (CMB) polarization anisotropies. We find that the amplitude of the lensing peak in the BB mode power spectrum is a faithful tracer of the dark energy dynamics at the onset of cosmic acceleration. This is due to two reasons. First, the lensing power is non-zero only at intermediate redshifts between the observer and the source, keeping record of the linear perturbation growth rate at the corresponding epoch. Second, the BB lensing signal is expected to dominate over the other sources. The lensing distortion on the TT and EE spectra do exhibit a similar dependence on the dark energy dynamics, although those are dominated by primary anisotropies.
We investigate and quantify the effect by means of exact tracking quintessence models, as well as parameterizing the dark energy equation of state in terms of the present value (w_0) and its asymptotic value in the past (w_∞); in the interval allowed by the present constraints on dark energy, the variation of w_∞ induces a significant change in the BB mode lensing amplitude. A Fisher matrix analysis, under conservative assumptions concerning the increase of the sample variance due to the lensing non-Gaussian statistics, shows that a precision of order 10% on both w_0 and w_∞ is achievable by the future experiments probing a large sky area with angular resolution and sensitivity appropriate to detect the lensing effect on the CMB angular power spectrum; the forecast precision reaches a few percent for highly dynamic models whose dark energy abundance at the epoch when lensing is most effective is sensibly larger than the present one, i.e. for $w_\infty \gtrsim$ -0.5. These results show that the CMB can probe the differential redshift behavior of the dark energy equation of state, beyond its average.

I. INTRODUCTION

One of the most challenging issues in modern cosmology is the comprehension of the nature of the dark energy, the unknown component representing about 70% of the cosmological critical density today, responsible for a late phase of acceleration in the cosmic expansion (see [1, 2] and references therein).
The first report on the evidence of cosmic acceleration was due to the magnitude-redshift relation inferred by type Ia supernovae [3, 4]; the cosmic microwave background (CMB) experiments, combined with the data on large scale structure, confirmed and strengthened that result (see [5] and references therein).
The simplest interpretation for the acceleration can be given in terms of a Cosmological Constant, leading however to serious theoretical problems concerning its magnitude. In fact, its energy scale is required to be 123 orders of magnitude lower than the Planck energy, possibly the only one relevant in the very early universe; and its value has to be such to render it comparable with the matter density at the present epoch. These issues are known as fine-tuning and coincidence, respectively (see e.g. [2]).
The concept of dark energy generalizes the Cosmological Constant, allowing dynamics of the equation of state and fluctuations of the dark energy component, in the attempt to alleviate these tweaking problems and to find clues to unveil the physical mechanism giving rise to the acceleration. This is the case of the Quintessence, a self-interacting scalar field evolving according to different potential energies. For reference, the potentials which have been studied extensively in the literature are characterized by an exponential shape [6], inverse power law [7], or a combination of those [8], and have been suggested in the context of particle physics beyond the standard model.
The present measurements are consistent with the Cosmological Constant case, $w = -1$ [9], with a precision of about ten percent. However, these observations do not have the capability to address the dynamics of the dark energy yet: the corresponding constraints either concern models where the dark energy is constant, or may be interpreted as constraints on the redshift average of the equation of state.
Most dark energy models, including the ones quoted above, may account for a present equation of state close to the Cosmological Constant case, but have a significantly different evolution

at the epoch of equality between dark matter and energy, occurring at redshift $z \simeq 0.5$. Therefore, on the basis of the Cosmological Constant problems, and having no other theoretical clue about the nature of the dark energy, it is clearly crucial to investigate its behavior at the onset of acceleration, where the models most differ.

The dark energy dynamics is and will be probed in the first place by the same observables which gave evidence for cosmic acceleration. The latest measurements of type Ia supernovae measurements are from space, from the Hubble Space Telescope (HST), reaching a redshift of about 0.5 [10]. With appropriate experimental resources, the type Ia supernovae measurements may get farther in redshift, collecting data from events occurred before the onset of acceleration, up to a maximum redshift between 1.5 and 2, thus probing the whole redshift interval where the dark energy is relevant [11]. At the same time, the combination of CMB and large scale structure probes the dark energy, through the modified history of structure formation. The local large scale structure is probed directly by the spatial distribution of galaxies. Indications on the cosmological structures at higher redshifts come from the distribution of the Lyα clouds [12]. The imprints of the baryon acoustic oscillations in the dark matter distribution have been observed [13]. In addition, the CMB undergoes a geometrical shift of the acoustic peak locations in the angular domain, because of the modified distance to the last scattering resulting from the change in the expansion rate. The 2dF survey [14] and Sloan Digital Sky Survey (SDSS, see [15] and references therein), and the CMB experiments culminating with the Wilkinson Microwave Anisotropy (WMAP, see [5] and references therein) contributed to set the quoted constraint on the dark energy equation of state [9]. On the other hand, as we stressed above, almost all those observables with the only exception perhaps of the baryon acoustic oscillations, rely on a line of sight integral of the light rays, picking up comparable contributions at all epochs from emission through observation; for those observables, the redshift behavior of the dark energy is averaged, and in particular markedly influenced by the expansion at recent epochs, where the observations require the dark energy to be close to a Cosmological Constant. In particular, the large scale structure survey data are mostly determined by nearby structures, only extending up to a redshift of about 0.1, while the CMB projection effect is dominated by the effect of the dark energy when it is most relevant, i.e. at the present. Therefore it is also important to study observables capable to pick up the dark energy abundance at the onset of acceleration. The lensing effect is a unique tool for this purpose, and is the subject of the present work. The reason is an elementary geometric property of lensing, yielding a null cross section if the lens position coincides with the observer or the source, thus probing intermediate regions only (see [16] for reviews).

The weak lensing in cosmology, i.e. the large scale shear injected on the background light by forming cosmological structures, is one of the most promising observables for future studies on dark matter and energy; a great effort is directed towards the study of the ellipticity induced by weak lensing on distant galaxies in the optical band, and how that is sensitive to the dark energy properties and other cosmological parameters. In principle, by measuring the weak lensing shear induced on shells of galaxies at different redshifts, either statistically or looking at the lensing induced by one single large structure, one has information on the redshift evolution of the dark energy abundance, which is equivalent to the knowledge of the equation of state dynamics [17, 18, 19]. In this perspective, a large experimental effort is ongoing; see [20] for reviews on the existing observations and future projects, [21, 22, 23] for parameter forecasts, also in connection with the constraints expected from other cosmological probes.

In particular, if the source can be considered at infinity the lensing cross section is non-zero at redshifts roughly between 0.1 and 10, peaking at $z \simeq 1$, rather independently of the particular cosmological model considered, and thus most relevant to study the universe at the corresponding epoch. This is the case of this work, where we consider the lensing of the CMB [24, 25, 26, 27, 28]. The relevance of CMB lensing as a tool for constraining the dark energy has been investigated for what concerns the statistics of order higher than the second for the anisotropies in total intensity [29, 30]. Indeed, even if the primordial CMB anisotropies obey a perfect Gaussian distribution, after lensing their statistics is modified as a result of the correlation among different scales induced by the lensing itself, in total intensity and polarization. Such effect appears already at the level of anisotropies in the total intensity, which represent the strongest component, and that is the reason why it has been studied so far mainly in that respect. As the present subject concerns the CMB lensing and is therefore related to that, we return on this issue in the concluding remarks.

Here we focus on a different domain where the

lensing is relevant for CMB, and precisely the anisotropy angular power spectrum, in particular for the the curl or BB component in the CMB polarization signal. The lensing re-distributes the primordial power and correlates different scales; as a result, the acoustic peaks in the total intensity (TT), gradient (EE) components of the CMB polarization and their correlation (TE) are smoothed, and some power is transferred from such scales to the damping tail. Moreover, a central aspect of the present work is that the gradient component of CMB polarization leaks into the BB modes, causing a broad peak centered on the angular scales of a few arcminutes, roughly corresponding to a multipole $l \simeq 1000$. Although the lowest expected contribution to the CMB anisotropies, this observable is entirely caused by lensing, and basically unbiased by primordial power; a contamination due to primordial gravitational waves may arise on larger angular scales, multipoles of about 100, where however the lensing signal is rapidly decreasing approaching the super-horizon regime. Furthermore, as we stated already, the lensing is a non-Gaussian process, correlating cosmological perturbations on different angular scales, while the primordial tensor power is expected to be close to Gaussianity. This difference might be crucial to deconvolve the two patterns [31]. The non-Gaussian distribution of lensing has an impact already at the level of the variance in the angular power spectrum of the BB modes, which is currently under investigation [33, 34, 35].
Therefore, since the lensing cross section is non-zero at intermediate redshifts only, as specified above, we do expect some relevance in studying this effect for investigating the dark energy at non-zero redshifts; in particular, being the BB power on the arcminute scale caused by lensing only, this relevance should be directly reflected by the behavior of that component. An analogous study, pointing out the lensing cross section redshift distribution and focusing on the high redshift dark energy behavior, has been performed considering the CMB third order statistics in total intensity anisotropies [29].

Our treatment is based on a previous work [36], casting the cosmological weak lensing theory in the context of scalar field dark energy models with arbitrary kinetic and potential forms in the fundamental Lagrangian, and also coupling arbitrarily to the Ricci scalar. The aim of that work was to embrace the most general scalar field dark energy models, including as a particular case the minimally coupled, purely self-interacting Quintessence, which is the scenario upon which this work is based. In section II we recall the relevant issues concerning the lensing computation in dark energy cosmologies. In section III we derive and discuss the lensed CMB power spectra and their dependence on the dynamical dark energy properties. In section IV we evaluate the impact on a parametric analysis of CMB data. Finally, in section V we draw our conclusions.

II. WEAK LENSING AND DARK ENERGY

In this section we describe the cosmological models we consider throughout this paper, and we outline the physics of lensing on the CMB total intensity and polarization anisotropies; for more details, see [36] and references therein. We focus on the modifications to the Boltzmann codes which numerically evolve cosmological perturbations required in order to take into account the effects of lensing in scalar field dark energy cosmologies.

A. Dark energy cosmology

In this paper we will consider the tracking Quintessence scenarios, where the dark energy is described through a scalar field ϕ (see e.g. [2]). The associated action is of the form:

$$S = \int d^4x\sqrt{-g}\cdot \cdot \left[\frac{1}{2\kappa}R - \phi^{;\mu}\phi_{;\mu}\frac{1}{2} - V(\phi) + \mathcal{L}_{\rm fluid}\right] . \quad (1)$$

We chose two representative models where the equation of state has a mild and violent redshift behavior, respectively for the inverse power law potentials, (IPL [7]) and those inspired by supergravity theories (SUGRA [8]):

$$V(\phi) = \frac{M^{4+\alpha}}{\phi^\alpha} \ , \ V(\phi) = \left(\frac{M^{4+\alpha}}{\phi^\alpha}\right) e^{4\pi G\phi^2} . \quad (2)$$

These scalar field dark energy models are implemented and integrated exactly, also considering Quintessence fluctuations, using DEfast, a modification of the Boltzmann code for numerical integration of cosmological background and linear perturbations based on the version 4.0 of CMBfast [41], which has been used in several papers, see [42, 43] and references therein.
For what concerns the background evolution, a variety of models including the ones above are well

described by essentially two parameters: those are the present value w_0 of the equation of state and its first derivative with respect to the scale factor a, $-w_a$ [44, 45]. In this framework, the evolution of the equation of state with the scale factor can be written as

$$w(a) = w_0 + w_a(1-a) = w_\infty + (w_0 - w_\infty)a \ , \quad (3)$$

where w_∞ is the asymptotic value of w in the past. We will exploit the parameterization above in Section IV, in order to evaluate the precision achievable on the measure of w_0 and w_∞ from the CMB total intensity and polarization angular power spectra.

B. Weak lensing and Boltzmann numerical codes in cosmology

The effect of gravitational lensing on the CMB spectra had been first introduced in the CMBfast code by Zaldarriaga and Seljak [28] for Cold Dark Matter (CDM) cosmologies including a Cosmological Constant (ΛCDM). In their formalism the effect on the correlation functions can be understood as the convolution of the unlensed spectra with a Gaussian filter determined by the *lensing potential* [16]. The expression for the lensing potential has to be generalized in scalar-tensor cosmologies because of the presence of anisotropic stress already at a linear level [36]. In the present scenario, however, this is not required and the structure of the quantities relevant for computing the lensing effect is formally unchanged.
Therefore, following the notation of the original paper [28], and showing for simplicity the TT case only, the anisotropy correlation between directions θ and θ', deflected by $\delta\theta$ and $\delta\theta'$, respectively, and separated by an angle θ is expanded in the harmonic space exploiting the flat sky approximation, taking the form

$$C_{TT}(\theta) = \int \frac{d^2\mathbf{l}}{(2\pi)^2} e^{il\theta\cos\phi_l} \langle e^{i\mathbf{l}\cdot(\delta\theta - \delta\theta')}\rangle C_{\tilde{T}\tilde{T}l} \quad (4)$$

where the expectation value in the above equation represents the ensamble average and is expressed as

$$\langle e^{i\mathbf{l}\cdot(\delta\theta-\delta\theta')}\rangle = e^{-\frac{l^2}{2}[\sigma_0^2(\theta) + \cos(2\phi_l)\sigma_2^2(\theta)]}, \quad (5)$$

and the quantities $\sigma_0^2(\theta)$ and $\sigma_2^2(\theta)$ are given by

$$\sigma_0^2(\theta) = 16\pi^2 \int_0^{\chi_{\rm rec}} W^2(\chi,\chi_{\rm rec}) d\chi \int_0^\infty k^3 dk \cdot \cdot P_\Phi(k, \tau = \tau_0 - \chi)[1 - J_0(k\theta\chi)] \ , \quad (6)$$

and

$$\sigma_2^2(\theta) = 16\pi^2 \int_0^{\chi_{\rm rec}} W^2(\chi,\chi_{\rm rec}) d\chi \int_0^\infty k^3 dk \cdot \cdot P_\Phi(k, \tau = \tau_0 - \chi) J_2(k\theta\chi) \ . \quad (7)$$

Here k is the wavenumber, J_l is the Bessel function of order l, χ is the comoving radial distance, τ is the cosmological conformal time, P_Φ is the power spectrum of the gravitational potential, and W is a function accounting for the cosmic curvature, which amounts to $1 - \chi/\chi_{\rm rec}$ for a flat universe. In ΛCDM cosmologies and most of the numerical codes dealing with them, including CMBfast, the quantities appearing in the above equations may be computed independently of the main routine which performs the integration of the hierarchical Boltzmann equations. This can be done because the power spectrum of matter density perturbations Δ_m can be factorized in two terms, depending respectively only on the wavenumber and the redshift:

$$P_{\Delta_m}(k,\chi) = Ak^n \cdot T^2(k,0) g^2(\chi) \ . \quad (8)$$

Ak^n here represents the primordial power, T is the transfer function of density perturbations taking into account the evolution on sub-horizon scales, and g is the perturbation linear growth factor. However, this separation is only convenient if one is provided with a satisfactory analytical fit of the growth of perturbations, which is not the case unless we ignore the influence of Quintessence perturbations, which do make a non-negligible effect on large scales [46]. To account for these changes, we evaluate numerically the gauge invariant expression of density perturbations from all fluctuating components Δ [47]. This quantity is computed and saved while the main routine performs the integration of the hierarchical Boltzmann equations, and used later for the numerical integration of the quantities (6) and (7), which include all fluctuating components.
A separate issue concerns the normalization constant A above when lensing is taken into account. The lensed perturbation spectra no longer depend linearly on the primordial normalization, since the lensing is a second order effect, being sourced by cosmological structures and acting on CMB anisotropies. Consequently, the description of the primordial anisotropy power has to be treated appropriately to take into account this occurrence; we modified our Boltzmann code in order to require the primordial normalization as an input, which is among the cosmological parameters to be constrained in Section IV.

This is different from the procedure followed in Section III, where we investigate phenomenologically the impact of lensing on the CMB angular power spectra as a function of the dark energy parametrization given above. The remaining parameters will be tuned to a fiducial value, in order to highlight differences and behavior induced exclusively by the variation of the underlying dark energy model; in particular, for the purposes of this Section only, the scenarios under examination are set to have the same amplitude of the primordial perturbations. An equivalent parametrization of the strength of primordial perturbations might be given with reference to the present epoch, usually by means of the variance evaluated on a scale of $8h^{-1}$ Mpc, σ_8; we choose the parametrization in terms of the primordial amplitude for numerical convenience, and we verify that the relevance of the effects we find does not depend on this choice.

III. LENSED CMB POLARIZATION POWER SPECTRA

We consider the two dark energy models discussed in the previous Section, as they well represent the different dynamics that the dark energy might have. We study the behavior of the relevant lensing quantities, showing results for the corresponding lensed CMB power spectra. In particular, we focus on the effect induced by the dark energy behavior at the epoch when the lensing power injection is effective. We give a qualitative description of how the lensing peak breaks the degeneracy between w_0 and w_∞ affecting the TT, TE and EE spectra, described later in detail.

Both the SUGRA and the IPL models are characterized by two parameters, the index of the power law α, and the mass of the field M. As it is well known [48, 49] they both admit attractor trajectories for the field dynamics in the early universe, known as tracking solutions. These are characterized by a relative independence of the field dynamics on its mass. The relevant parameter ruling the motion of the field is α, which in our example is set respectively as -2.21 and -0.34 for the SUGRA and IPL models. On the other hand, the mass sets the normalization of the dark energy density along the trajectory, being therefore crucial to achieve acceleration today, and must be set accordingly.

First of all we want to discuss qualitatively the effects on the corresponding background evolution, where we expect to see the most relevant differences between the two models; the key point of the comparison is the behavior of the dark energy component, which will characterize the scaling of the expansion factor. We consider models where the present equation of state of the dark energy is $w_0 = -0.9$, consistently with the present constraints [9]. The redshift evolution of $w(z)$ is shown in Fig. 1, showing that while in the IPL model it is mildly departing from its present value at high redshifts, in the SUGRA one it rapidly gets to higher values. The different behavior of the dark energy density affects of course directly H^2, which is also plotted relatively to the two models in the figure; the difference peaks between redshift 1 and 2, and then quickly decreases, due to the increasing matter dominance. The remaining cosmological parameters are chosen accordingly to the concordance ΛCDM model, listed in the first column of table I.

Since in the SUGRA model the dark energy keeps being relevant at higher redshifts with respect to the IPL case, the inhibition of structure formation starts earlier (see [50] and references therein);

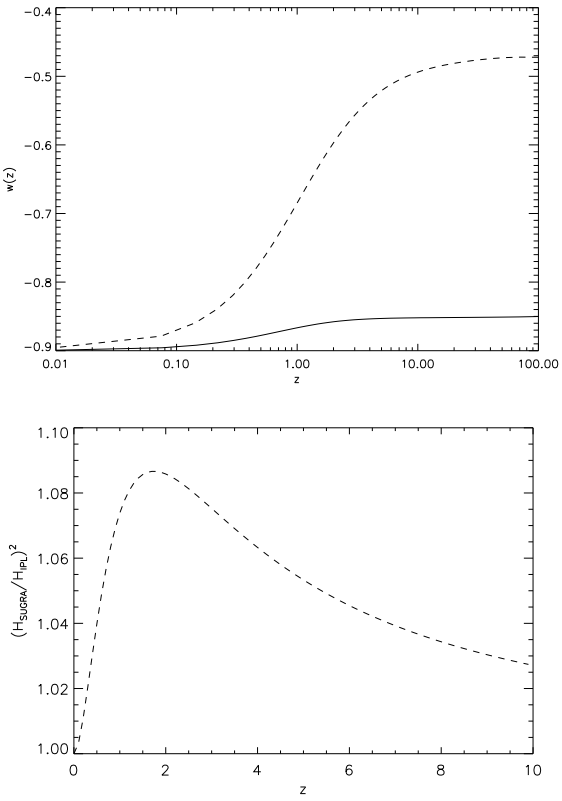

FIG. 1: Top: evolution of the equation of state of dark energy for the SUGRA (dashed line) and IPL (solid line) models. Bottom: ratio of H^2 in the two models as a function of redshift.

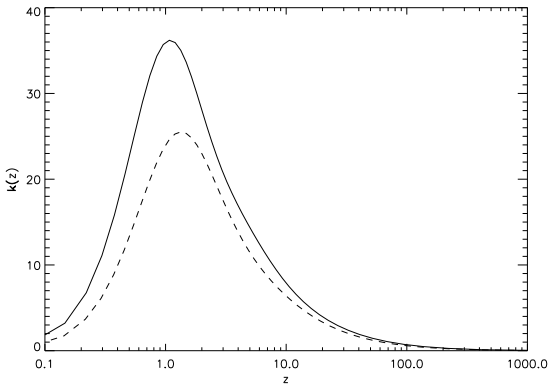

FIG. 2: Lensing kernel for $\theta = 4 \cdot 10^{-3}$ rad, for the SUGRA (dashed line) and IPL (solid line) models, having the same equation of state today.

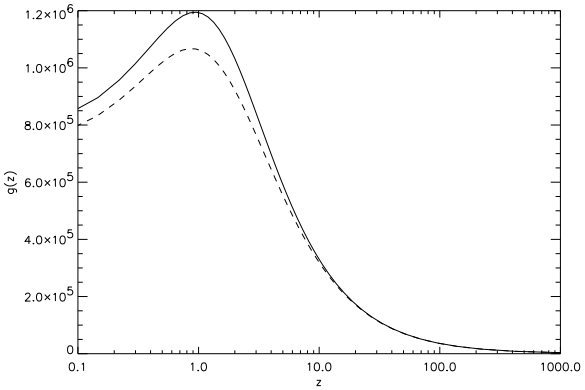

FIG. 3: Growth factor of the perturbations for a comoving wavenumber $k = 0.1$ Mpc^{-1}, for the SUGRA (dashed line) and IPL (solid line) models. In the two models, g has the same value at infinity.

thus, for a fixed primordial normalization, we expect two effects. The first is a smaller lensing signal in the SUGRA case, where clustering suppression starts earlier. The second is that the redshift interval where the lensing signal picks up its power, formally defined here below, is shifted towards earlier epochs, as a consequence of the structure formation process occurring at higher redshifts following the earlier dark energy dominance. These features can be verified analyzing the redshift behavior of the function which appears in the integral defining $\sigma_0(\theta)$; we choose a reference value of the angle, say $\theta_0 = 4 \cdot 10^{-3}$ radians, corresponding roughly to the middle of the range suitable for CMB computations. We consider the function $k(\theta_0, z)$, which gives σ_0^2 in (6) when integrated over z, assuming an unitary power spectrum for the gravitational potential fluctuations. We call the resulting quantity the *lensing kernel*; its dimensions are the inverse of a volume, and it gives a measure of the redshift distribution of the lensing effect coming from the background cosmological expansion. The result is shown in Fig. 2. Both our expectations are verified; note how the two cosmological models, although having the same values of all cosmological parameters today, differ substantially (30%) at the peak entirely because of the behavior of the dark energy equation of state. The corresponding behavior for the function giving σ_2^2 when integrated over z, evaluated on the same scale and using an unitary power spectrum, is qualitatively similar; indeed, the relevant quantity is $W^2 = (1 - \chi/\chi_{\rm rec})^2$, appearing multiplied by functions vanishing at present in the integral of both (6) and (7).

Let us now turn to analyze the impact of the different perturbation growth rate, influencing $\sigma_0(\theta)$ and $\sigma_2(\theta)$ through the power spectrum of the gravitational potential. It is convenient to plot the linear growth factor, $g(\tau)$, for the two models at a fixed wavenumber; the behavior is qualitatively the same for any κ. The result is shown in Fig. 3. The phenomenology is the following. In the matter dominated era, say at redshifts between 1000 and a few in the figure, g has the well known scaling as $a = 1/(1+z)$. At the onset of acceleration, its growth is inhibited and eventually it starts to decrease. As expected, this effect is stronger in the SUGRA case, as dark energy dominance takes place earlier. We also notice that the relation between the curves in Fig. 3 is similar to the ones in 2: the case of SUGRA has less power with respect to the IPL. This brings us to fix the quantity which matters here, i.e. causing the differences we just discussed. That is simply the dark energy abundance at the epoch in which lensing injects its power, corresponding to the interval outlined by the lensing kernel in Fig. 2. Indeed, the latter as well as the perturbation growth rate are determined by the Hubble expansion rate, which contains the dark energy through the Friedmann equation. The higher is the dark energy, the higher H, causing an higher suppression of perturbations, Fig.3, as well as modified geometry, Fig.2. Unfortunately, there is no unique parameter fixing the dark energy abundance at a given redshift, which is determined in general by the present abundance and $w(z)$; in our parametrization, usually the most relevant parameter is w_∞, specifying the dark energy density redshift behavior at high redshifts,

but only approximately in models where w_∞ is sensibly larger than w_0. On the other hand, the improvement from having the lensing effect in the CMB analysis is evident keeping the parametrization we have exploited so far, as we show in the following. As a final remark of this part of the discussion, we notice that the the combination of the two effects of background evolution and perturbations growth contributing to the expressions of σ_0 and σ_2 is indeed large. We thus expect a significant dependence of the amplitude of CMB lensing power upon the dark energy equation of state value in the redshift interval which is relevant for lensing, i.e. the one outlined by the lensing kernel in Fig. 2.

On the basis of the issues outlined above, it is crucial to fix CMB observables purely sourced by gravitational lensing. The BB modes in the CMB represent an almost ideal candidate for this, since the lensing dominates their power on sub-degree angular scales. In the following we give a qualitative illustration of their relevance, leaving a more quantitative discussion for the next Section.

The TT, TE and EE CMB spectra are dominated by primary anisotropies, imprinted at last scattering, where in most models the dark energy is not yet effective. The location of the acoustic peaks depends on the different cosmological expansion histories, as a result of the modification in the comoving distance to last scattering d_{LS}, which is written as

$$d_{LS} = H_0^{-1} \int_0^{z_{LS}} dz[\Omega_m(1+z)^3 + \\ +(1-\Omega_m)e^{3\int_0^z dz' \frac{1+w(z')}{1+z'}}]^{-1/2} . \qquad (9)$$

where H_0 is the Hubble parameter, Ω_m is the matter abundance today relative to the critical density and the contributions from radiation and curvature are neglected. It does not come as a surprise that this quantity depends very weakly on different forms of $w(z)$, since those are washed out by two integrals in redshift; the latter occurrence gives rise to the so-called projection degeneracy of CMB anisotropies. This simply comes from the fact that d_{LS} is the same for different combinations of parameters in (9); in particular, for a given set of those except the dark energy equation of state, there is an entire set of curves $w(z)$ giving rise to the same d_{LS}; in general, in all those models the dark energy is negligible at decoupling, so that the shape of acoustic peaks is also unchanged, making the spectra in those models nearly identical, and therefore degenerate. The Integrated Sachs-Wolfe effect (ISW) acts on large scales only, responding to the change in the cosmic equation of state; although promising results may be obtained correlating the ISW with the large scale structure data [51], from a pure CMB point of view the cosmic variance represents a substantial limiting factor.

The BB phenomenology is utterly different. Here the lensing is the only source of power on sub-degree angular scales, and the lensing cross section is largest at intermediate redshifts, say around $z \simeq 1$ as Fig. 2 shows, where the dark energy might differ significantly from a Cosmological Constant, even for the same expansion rate today. The lensed CMB power spectra are shown in Figs. 4, 5, 6. The TT, TE and EE spectra undergo a projection effect due to the modified distance to last scattering, plus a lensing distortion which is barely visible, as the curves are still dominated by the primordial component of anisotropies. On the other hand, the BB spectrum amplitude is markedly affected by the different lensing process in the two models. Indeed, as we discussed above, the BB peak directly traces the perturbation growth rate and the background expansion in the redshift interval visible in Fig. 2. For the cosmological parameters at hand, the effect is of 20-30 percent, consistently with the results in Figs. 2, 3. We remark that the C_ls have been obtained with the same value of all cosmological parameters, including the primordial normalization, and differ only in the value of the dark energy equation of state at redshifts relevant for lensing. As we explained above, that is equivalent to a different dark energy abundance between the models considered at that epoch, and therefore a different expansion rate, which determines the strength of the lensing process. In order to check that the magnitude of the effect we point out does not depend on the normalization procedure adopted, in Fig. 7 we plot the BB lensing peak for the SUGRA and IPL models, normalized to have the same σ_8 at present, which is chosen to be 0.844. Correspondingly, the models need now to start from a different primordial normalization, in order to get the same present power, given their different perturbation growth histories represented in Fig. 3. As it is evident, the magnitude of the difference is comparable to the one in Fig. 6, but the order of the curve is reversed. This may be understood by looking again at Fig. 3; starting from the same power at present, and going towards higher redshifts, in the SUGRA model perturbations are higher at any epoch, determining the opposite behavior with respect to Fig. 6. Thus, the fact that the lensing difference is comparable in both cases

makes us confident that the effect we point out is not an artefact of the normalization procedure.

We now demonstrate how the lensing breaks the projection degeneracy mentioned above. For simplicity, here and in the rest of this Section we adopt the simple parametrization in terms of w_0 and w_∞. Let's consider dark energy models featuring the same value of d_{ls} in (9), with different values of w_0 and w_∞. The TT and BB spectra are shown in Figs. 8 , 9, showing clearly the same pattern in the TT acoustic peaks but markedly different BB amplitude, reflecting the enhanced dependence of the latter on w_∞. It is appropriate here to make a connection with the issue outlined before of the relevance of the dark energy abundance through H. The dark energy density at the epoch which is relevant for lensing, see Fig.2 again, follows an opposite behavior with respect to the curves represented in the figure: the lower the curve, the higher the value of the expansion rate at the lensing relevant epoch leading to an increasing suppression of the power, the higher the dark energy density at the corresponding redshifts, which is mainly influenced by w_∞ here, as the present dark energy abundance is the same.

Finally, we wish to address an important point which will be relevant in the next Section, i.e. the lensing distortion on the TT, TE and EE modes. Indeed, most of the reasoning exposed in this Section, represented by the phenomenology in Figs. 2 and 3, does not apply to the lensing BB modes only, but to every effect coming from lensing. It is therefore relevant to compare the lensing effect on non-BB modes, too. This is done in Fig. 10, where we plot the quantity $(C^{XX}(w_\infty + dw_\infty) - C^{XX}(w_\infty))/C^{XX}(w_\infty)$, where XX stays for TT, EE and BB. Such quantity represents the fractional change to the spectra induced by a different dark energy abundance at the epoch in which the lensing is active, see Fig. 2 again; the latter is determined entirely by w_∞, as w_0 is fixed to -1, and the present dark energy abundance is the same. We perform a double-sided variation around the ΛCDM cosmology, so that $w_\infty = -1$, and $dw_{\infty=0.05}$. As it is evident, the changes have a comparable order of magnitude for all the spectra, including the BB one; remarkably, the latter is not oscillating around zero, but possesses a definite sign. This is due to the absence of sharp peaks and valleys in the spectrum, which in turn comes from the lensing capability of correlating different scales, smearing out the EE peaks which represent the source for BB lensing modes. That may be a relevant aspect for experiments looking at limited sky patches, for which a binning procedure is required. The binning would of course reduce the relevance of the lensing distortion on the TT and TE, while the BB would remain substantially unaffected.

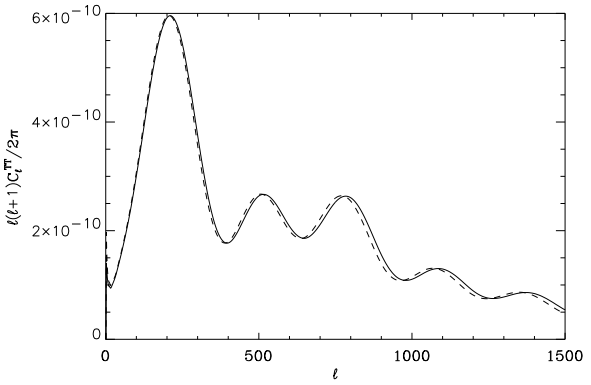

FIG. 4: TT lensed power spectra for the SUGRA (dashed line) and IPL (solid line) models.

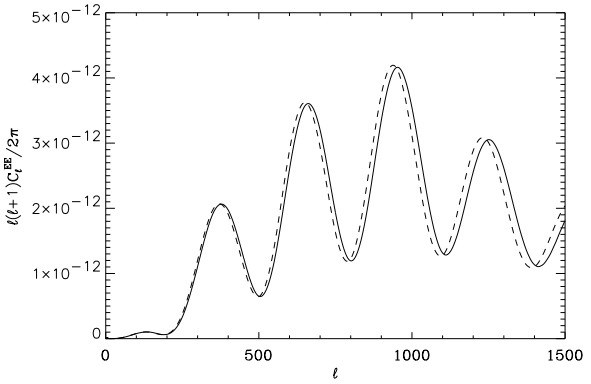

FIG. 5: EE lensed power spectra for the SUGRA (dashed line) and IPL (solid line) models.

In the next Section, we will evaluate the relevance of considering the lensing effect for cosmological parameter estimation.

IV. FISHER MATRIX ANALYSIS

Here we give a first quantitative evaluation of the benefit that the knowledge of the lensing and in particular the BB spectra has on the CMB capability of constraining the dark energy dynamics. Our approach is based on a Fisher matrix analysis, reviewed in Section IV A; in Section IV B we show the results.

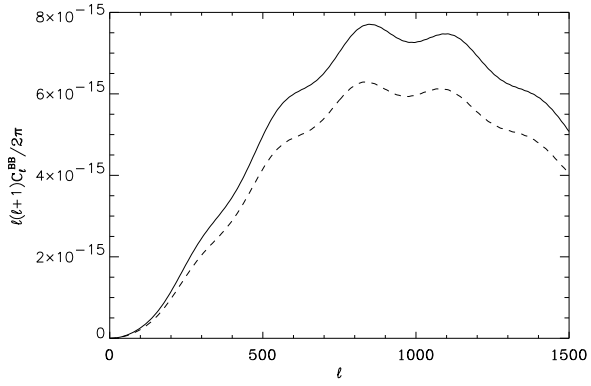

FIG. 6: BB lensed power spectra for the SUGRA (dashed line) and IPL (solid line) models.

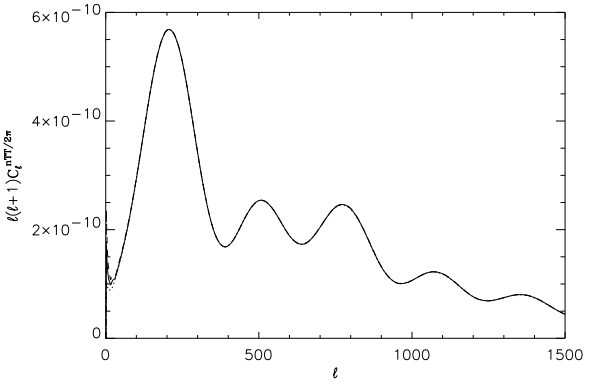

FIG. 8: Lensed TT power spectra for dark energy models with $w_0 = -0.9$, $w_\infty = -0.4$ (solid line), $w_0 = -0.965$, $w_\infty = -0.3$ (dashed line), $w_0 = -0.8$, $w_\infty = -0.56$ (dotted line).

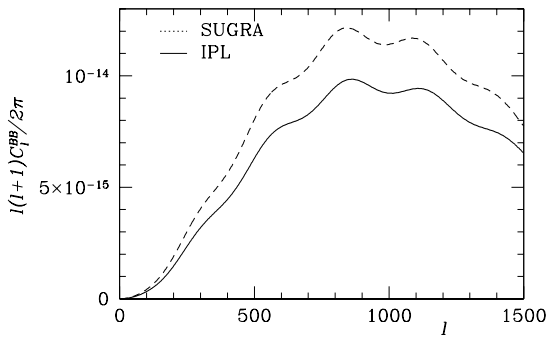

FIG. 7: Lensed BB power spectra for the IPL and SUGRA models, normalized to have the same σ_8 at present.

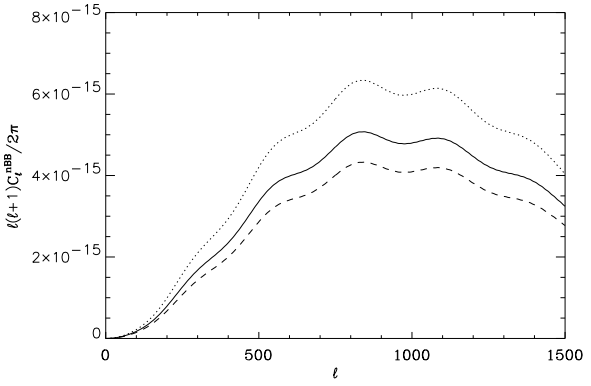

FIG. 9: Lensed BB power spectra for dark energy models with $w_0 = -0.9$, $w_\infty = -0.4$ (solid line), $w_0 = -0.965$, $w_\infty = -0.3$ (dashed line), $w_0 = -0.8$, $w_\infty = -0.56$ (dotted line).

A. Method

In a CMB analysis involving the polarization power spectra [52], the Fisher matrix takes the form

$$\mathrm{F}_{ij} = \sum_\ell \sum_{XY} \frac{\partial C_\ell^X}{\partial \alpha_i} \left[\Xi_\ell\right]^{-1}_{XY} \frac{\partial C_\ell^Y}{\partial \alpha_j}, \qquad (10)$$

where X and Y are either TT, EE, TE or BB and $\Xi_{XY} \equiv \mathrm{Cov}(C_\ell^X C_\ell^Y)$ is the power spectra covariance matrix:

$$\Xi_\ell = \begin{pmatrix} \Xi_\ell^{TT,TT} & \Xi_\ell^{TT,EE} & \Xi_\ell^{TT,TE} & 0 \\ \Xi_\ell^{TT,EE} & \Xi_\ell^{EE,EE} & \Xi_\ell^{EE,TE} & 0 \\ \Xi_\ell^{TT,TE} & \Xi_\ell^{EE,TE} & \Xi_\ell^{TE,TE} & 0 \\ 0 & 0 & 0 & \Xi_\ell^{BB,BB} \end{pmatrix}. \qquad (11)$$

The terms in the power spectra covariance matrix are given by

$$\begin{aligned} \Xi_\ell^{xy,x'y'} &= \frac{1}{(2\ell+1) f_{sky} \Delta\ell} \\ &\times \left[(C_\ell^{xy'} + N_\ell^{xy'})(C_\ell^{yx'} + N_\ell^{yx'}) \right. \\ &\left. +(C_\ell^{xx'} + N_\ell^{xx'})(C_\ell^{yy'} + N_\ell^{yy'})\right] \qquad (12) \end{aligned}$$

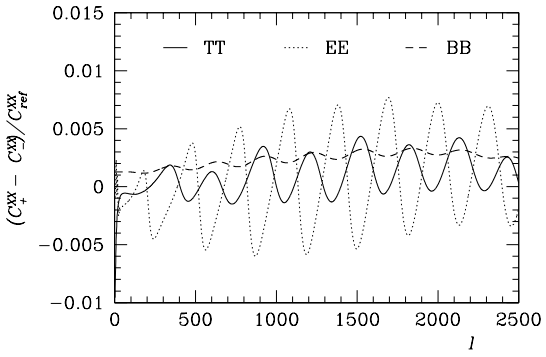

FIG. 10: Relative lensing changes for the TT, EE and BB CMB spectra, varying around a ΛCDM cosmology.

where $(x, y) = (T, E, B)$. The noise covariance is given by N_ℓ^{xy}, which also contains the effect of the instrumental beam, assumed Gaussian and circular. The inverse of the Fisher matrix gives the uncertainty on the theoretical parameters:

$$\mathcal{C}_{ij} \equiv \langle \Delta\alpha_i \Delta\alpha_j \rangle = \mathrm{F}_{ij}^{-1} \ . \tag{13}$$

$\Delta\alpha_i$ is the marginalized 1-σ error on the $i^{\rm th}$ parameter, and is given by the square root of the diagonal elements of the inverse of the Fisher matrix.

As a representative of the forthcoming CMB polarization probes capable to detect the BB spectrum we consider a post-Planck all-sky experiment. We conservatively consider a Gaussian beam with 7 arcminutes full width half maximum, considering multipoles up to $l = 1800$. We assume an instrumental error of 1 μ K on the beam scale, and cut the galactic plane assuming a sky fraction of 0.66.

A delicate issue in applying a Fisher matrix analysis to the CMB lensing is represented by the non-Gaussianity of the lensing effect, due to the correlation of cosmological perturbations on different angular scales; the lensing statistics is being investigated, receiving increasing attention in view of the incoming precision polarization experiments [31, 33, 34, 35, 53].

In particular, Smith et al. [34] achieved a first quantification of the increase in the covariance matrix due to the non-Gaussian nature of the lensing signal in the BB modes, giving a pipeline to estimate the resulting achievable accuracy.

For our study their most relevant result is the behavior of the so called *degradation factor*, the ratio between the squared sample covariance in the case of this non Gaussian signal and the corresponding Gaussian case. This is shown to depend both on the instrumental error (the degradation increases with the signal-to-noise ratio of the experiment, as expected because the instrumental error is close to Gaussian) and on the maximum available multipole (again increasing with l_{max}, because of the stronger effect of the correlation between neighboring band powers).

According to their worst case scenario, we make a conservative choice enlarging by a factor 10 the covariance contribution to the BB spectrum in the covariance matrix (12); this would correspond to an experiment with $l_{\rm max} = 2000$ and $\theta_{\rm FWHM} \simeq 1'$.

Steps further in the issue of taking into account has been made in [32], who suggested a way of taking into account the non-Gaussian correlations of the lensed BB spectra,with special regard on the issue of degeneracies between the dark energy parameters and the neutrino mass, and most recently in [53]. These approaches go however beyond the scope of the present paper, and may be considered in further work.

TABLE I: Results from the Fisher matrix analysis for the ΛCDM and the IPL models.

	ΛCDM		**IPL**	
	value	σ_{Fisher}	value	σ_{Fisher}
w_0	$-1.$	0.12	-0.9	9.7×10^{-2}
w_∞	$-1.$	0.27	-0.8	0.19
$\Omega_b h^2$	0.022	5.7×10^{-5}	0.022	6.0×10^{-5}
$\Omega_C h^2$	0.12	7.0×10^{-4}	0.12	7.3×10^{-4}
h	0.72	5.0×10^{-2}	0.72	4.5×10^{-2}
n_S	0.96	2.1×10^{-3}	0.96	2.2×10^{-3}
τ	0.11	3.1×10^{-3}	0.11	3.0×10^{-3}
A_S	1.0	5.6×10^{-3}	1.0	5.5×10^{-3}

B. Marginalized errors on cosmological parameters

We analyze four cosmological models, corresponding to a pure ΛCDM, and inverse power law, and two SUGRA cases, specified by eight cosmological parameters, including the two specifying the dark energy equation of state:

TABLE II: Results from the Fisher matrix analysis for two SUGRA models.

	SUGRA1		**SUGRA2**	
	value	σ_{Fisher}	value	σ_{Fisher}
w_0	-0.9	6.1×10^{-2}	-0.82	3.5×10^{-2}
w_∞	-0.4	6.9×10^{-2}	-0.24	1.9×10^{-2}
$\Omega_b h^2$	0.022	5.7×10^{-5}	0.022	5.9×10^{-5}
$\Omega_C h^2$	0.12	6.6×10^{-4}	0.12	5.0×10^{-4}
h	0.72	2.9×10^{-2}	0.72	1.5×10^{-2}
n_S	0.96	2.1×10^{-3}	0.96	2.0×10^{-3}
τ	0.11	3.1×10^{-3}	0.11	3.2×10^{-3}
A_S	1.0	5.5×10^{-3}	1.0	5.6×10^{-3}

w_0	present e.o.s. of dark energy
w_∞	asymptotic past e.o.s. of dark energy
h	present value of Hubble parameter
$\Omega_{\rm B} h^2$	fractional baryon density $\times\, h^2$
$\Omega_{\rm C} h^2$	fractional CDM density $\times\, h^2$
$A_{\rm S}$	primordial normalization parameter
$n_{\rm S}$	perturbation spectral index
τ	reionization optical depth

All the cosmological parameters, are chosen consistently with the current observations of CMB and large scale structure [9]; of course the dark energy equation of state is allowed to depart from a ΛCDM case. We assume the same values for the non-dark-energy parameters for all the models. Their values are listed in the first and third column of the Tabs. I, II. As we specified in the previous Section, in our numerical machinery the normalization is performed through an input parameter specifying the primordial power. For all the four reference models we run DEfast with the inbuilt large-scale normalization option (COBEnormalize), we correct in order to reproduce the best fit of the combined datasets of WMAP 1st year, CBI and ACBAR (see [5] and references therein), and we use these four numbers as the reference primordial amplitudes for each model. The parameter A_S is the ratio of the primordial amplitude with respect to the latter; this is done for notational convenience since the units of DEfast, based on version 4.1 of CMBfast, are not easily interpreted in terms of physical quantities. The value $A_S = 1$, reported for the four cases, does not therefore indicate that the models have the same amount of primordial perturbations, but simply that for each case the adopted normalization is the one obtained with the procedure described above, whose actual value is, of course, model-dependent. Indeed all the models give rise to a similar value for σ_8, which is $\simeq 0.86$ for the ΛCDM case and $\simeq 0.81$ for the highly dynamical SUGRA2.

The results of the analysis are shown in the second and fourth column of tables I, II, reporting the $1-\sigma$ marginalized errors for each parameter, according to the present Fisher matrix approach. For the ΛCDM model there is an important indication of an achievable precision smaller than 20% on the w_0 parameter, while the limit on w_∞ is considerably weaker. The accuracy on the others is in agreement with previous similar analysis [54], which was indeed expected because the BB modes statistics have large error bars and trace the physics at late redshifts so that their influence on other parameters is smaller. Results are increasingly better for the IPL and the two SUGRA cases; this can be attributed to the more and more violent redshift behavior of the equation of state of these models, making them increasingly sensitive to the redshift region probed by lensing, outlined in Fig. 2. In particular, the achievable precision on the w_∞ parameter appears to be growing faster, so that for the SUGRA cases the results for the two dark energy parameters are comparable.

As we did in the discussion in the last part of the previous Section, it is relevant to evaluate the role of the BB modes compared to the lensing distortion on the TT, TE and EE spectra. When the lensing effect is not considered, i.e. performing an analysis only on the unlensed $\mathcal{C}^{TT}$, $\mathcal{C}^{TE}$ and $\mathcal{C}^{EE}$ spectra, the projection degeneracy related to the last scattering surface distance (9) is almost exact making in particular the Fisher matrix singular. When the lensing is taken into account, even on the spectra which are actually dominated by the primordial power, namely the TT, TE and EE ones, such degeneracy is broken, as Fig. 10 proves. It is interesting to compare the forecast precision on the cosmological parameters we consider, in particular w_0 and w_∞, in presence of absence of the lensing BB modes. Looking at Fig. 10, we roughly expect a precision increase of order 20% in the w_∞ parameter, as the order of magnitude of the relative variation in the BB power is of the order of the other ones. The results are shown in tables III and IV and confirm our expectation, in some cases being even larger than the naive ex-

pectation due to the peculiar sensitivity of the BB modes spectrum to the dark energy equation of state derivative. It is also interesting to note that there are significant improvements in the precision on some of the remaining parameters as well, as a result of the addition of a new independent observable.
In the next Section we further comment these results, and draw our conclusions.

TABLE III: Results from the Fisher matrix analysis in absence or presence of the BB modes.

	ΛCDM		**IPL**	
	σ (no BB)	σ (with BB)	σ (no BB)	σ (with BB)
w_0	0.13	0.12	0.11	9.7×10^{-2}
w_∞	0.31	0.27	0.24	0.19
ω_B	6.4×10^{-5}	5.7×10^{-5}	6.5×10^{-5}	6.0×10^{-5}
ω_C	7.9×10^{-4}	7.0×10^{-4}	7.8×10^{-4}	7.3×10^{-4}
h	5.6×10^{-2}	5.0×10^{-2}	5.4×10^{-2}	4.5×10^{-2}
n_S	2.3×10^{-3}	2.1×10^{-3}	2.3×10^{-3}	2.2×10^{-3}
τ	3.2×10^{-3}	3.1×10^{-3}	3.0×10^{-3}	3.0×10^{-3}
A_S	5.7×10^{-3}	5.6×10^{-3}	5.6×10^{-3}	5.5×10^{-3}

TABLE IV: Results from the Fisher matrix analysis in absence or presence of the BB modes.

	SUGRA1		**SUGRA2**	
	σ (no BB)	σ (with BB)	σ (no BB)	σ (with BB)
w_0	$0.6.6 \times 10^{-1}$	6.1×10^{-2}	3.7×10^{-2}	3.5×10^{-2}
w_∞	7.9×10^{-2}	6.9×10^{-2}	2.1×10^{-2}	1.8×10^{-2}
ω_B	6.4×10^{-5}	5.7×10^{-5}	6.5×10^{-5}	5.9×10^{-5}
ω_C	7.5×10^{-4}	6.6×10^{-4}	7.0×10^{-4}	5.0×10^{-4}
h	3.3×10^{-2}	2.9×10^{-2}	1.6×10^{-2}	1.5×10^{-2}
n_S	2.2×10^{-3}	2.1×10^{-3}	2.3×10^{-3}	2.0×10^{-3}
τ	3.2×10^{-3}	3.1×10^{-3}	3.2×10^{-3}	3.2×10^{-3}
A_S	5.8×10^{-3}	5.5×10^{-3}	6.0×10^{-3}	5.6×10^{-3}

V. CONCLUSIONS

Our aim in this paper is to study the potentiality of the CMB physics, with particular regard to the BB modes of the polarization, which are sourced by gravitational lensing of cosmic structures, in order to constrain the dark energy dynamics at the epoch of equivalence with the non-relativistic matter component. We focus on the lensing effect and in particular on the amplitude of the BB angular power spectrum; BB mapping techniques isolating the lensing power [31] might also be considered for extracting information about the cosmic expansion rate redshift behavior. We have shown how the CMB lensing, being directly linked to the cosmic dynamics and linear perturbation growth rate when the dark-energy enters the cosmic picture, presents an enhanced sensitivity to the value of the dark energy equation of state at the corresponding epoch. Such a feature breaks the so called projection degeneracy, affecting the unlensed spectra, preventing the possibility of constraining the redshift dependence of the dark energy equation of state from CMB. These features are particularly evident by looking at the response of the amplitude of the BB angular power spectrum induced by lensing; the latter is lowered by a factor as large as 30% if the equation of state of the dark energy at high redshifts is raised to the value of typical Quintessence models, currently allowed by observations; correspondingly, the TT, TE, EE spectra undergo an angular shift in the acoustic peaks location, and a variation in the the smearing of acoustic peaks because of lensing. The reasons are that, on one hand, the lensing probes only intermediate redshifts between source and observers, and on the other, that the lensing dominates the BB power. The first aspect is clearly not specific to the CMB angular power spectrum, but may applied to any CMB lensing observable. Analogous studies have been focused on the non-Gaussian power injection into the anisotropy statistics of order larger than the second [29, 30]. Indeed, the outcome of these studies is consistent with the present one, i.e. the lensing power in the CMB bispectrum, the harmonic space analogue to the three point correlation function, presents a remarkable sensitivity to the dark energy equation of state at the onset of acceleration. Thus the present study is related to those, although on a completely different domain. Since we still don't know where the impact of instrumental systematics and foregrounds will be the strongest in a real experiment attempting to detect the CMB lensing signal, it is important to carry out the analysis on all CMB lensing observables, and in particular on the angular power spectrum. Our results show that the relative changes, $\delta C_l^{XY}/C_l^{XY}$ where XY stays for TT, EE, TE or BB, induced by lensing are all of the

same order of magnitude, but in addition there are at least two reasons why the BB signal should be taken into account. First, the BB modes in CMB polarization at the arcminute scale are the explicit target of forthcoming CMB probes (see ie [56] and references therein). Second, their response to the variation of the dark energy abundance has a definitee sign, while the others oscillate around zero; this might cause a difference in favour of the lensing BB modes for experiments targeting a limited fraction of sky, due to the potential loss of information involved in the binning procedure.

We have then quantified the scientific impact of our result in terms of the achievable precision on the cosmological parameters, evaluated through a Fisher matrix analysis, modeling our assumptions on the specifics of forthcoming probes of CMB polarization, for Cosmological Constant and three more dynamical dark energy scenarios. The results are strongly encouraging, predicting an accuracy better of order 10% on the present value of the dark energy equation of state, and a somehow weaker limit on its first derivative with respect to the scale factor, but with an important indication of better results with increasing dark energy dynamics. The inclusion of the BB spectra is responsible at the 10 to 20 percent level for the quoted forecasts. This result is comparable with the one quoted in [22], where the authors take into account SNIa data and CMB physics but do not include BB modes into the analysis and with the forecasts in [21] for Quintessence models, where the authors consider SNIa data and weak lensing of background galaxies. In particular, the prediction of a smaller uncertainty for high dark energy dynamics is reproduced also for the observable considered here. The latter might be a complementary and independent dark energy probe with respect to the ones mentioned above. In [55], a work which came out in the literature during the refereeing process of the present one, the lensing BB modes are included in the analysis, finding a benefit which is similar to the one found here.

In conclusion, the weak lensing of the CMB is confirmed by this work as a potential probe of the dark energy dynamics when acceleration starts, independently of the present expansion rate. This adds even more interest to the impact of high precision weak lensing measurements in cosmology [20]. Moreover, our results indicate that the measure of the dark energy dynamics suggested here could be achieved by the forthcoming CMB probes aiming at the detection of the polarization BB modes.

VI. ACKNOWLEDGMENTS

We thank Julien Lesgourgues, Samuel Leach, Matias Zaldarriaga and Matthias Bartelmann for useful conversations and suggestions. This research was in part supported by the NASA LTSA grant NNG04GC90G.

[1] T. Padmanabhan, *Phys. Rep.* **380**, 235 (2003).
[2] P.J.E. Peebles, B. Ratra *Rev. Mod. Phys.* **75**, 559 (2003).
[3] S. Perlmutter et al., *Astrophys. J.* 517, 565 (1999).
[4] A. G. Riess et al., *Astrophys. J.* 116, 1009 (1998).
[5] D. N. Spergel et al., *Astrophys. J. Supp.* **148**, 97 (2003).
[6] C. Wetterich, *Nucl. Phys.* B **302**, 668 (1988).
[7] B. Ratra and P.J.E. Peebles, *Phys. Rev. D* **37**, 3406 (1988).
[8] P. Brax and J. Martin, *Phys. Rev. D* **61**, 103502 (2000).
[9] U. Seljak, A. Slozar, P. McDonald, astro-ph/0604335 (2006)
[10] A. Chiocchiatti et al., *Astrophys. J.* in press, astro-ph/0510155 (2006).
[11] E.V. Linder for the SNAP collaboration, *Astronomical Society of the Pacific*, **339**, 87 (2005).
[12] M. Viel, M.G. Haenhelt, A. Lewis, *MNRAS Lett.* **360**, 51 (2006).
[13] D.J. Eisenstein et al., *Astrophys. J.* **633**, 560 (2005).
[14] S. Cole et al., *MNRAS* **363**, 505 (2005).
[15] U. Seljak et al., *Phys. Rev. D* **71**, 103515 (2005).
[16] M. Bartelmann and P. Schneider, *Phys. Rep.* **340**, 291 (2001).
[17] W. Hu, B. Jain, *Phys. Rev. D* **70** 043009 (2004).
[18] B. Jain, A. Taylor, *Phys. Rev. Lett.* **91**, 141302 (2003).
[19] W. Hu, *Phys. Rev. D* **66**, 083515 (2002).
[20] A. Refregier, *Ann. Rev. Astron. Astrophys.* **41**, 645 (2003).
[21] J. Albert et al. for the SNAP collaboration, astro-ph/0507460 (2005).
[22] Ch. Yeche et al., astro-ph/0507170 (2005).
[23] Y.-S. Song, L. Knox, *Phys. Rev. D* **70**, 063510 (2004).
[24] A. Lewis, A. Challinor, astro-ph/0601594 (2006).
[25] W. Hu, *Phys. Rev. D* **64**, 083005 (2001).
[26] W. Hu, *Phys. Rev. D* **66**, 043007 (2000).
[27] D.M. Goldberg, D.N. Spergel *Phys. Rev. D* **59**, 103002 (1999).
[28] M. Zaldarriaga and U. Seljak, *Phys. Rev. D* **58**,

023003 (1998).
[29] F. Giovi, C. Baccigalupi, F. Perrotta, *Phys. Rev. D* **71**, 103009 (2005).
[30] L. Verde, D.N. Spergel, *Phys. Rev. D* **65**, 043007 (2002).
[31] C. Hirata and U. Seljak, *Phys. Rev. D* **68**, 083002 (2003).
[32] S. Smith, A. Challinor and G. Rocha, astro-ph/0511703 (2005).
[33] Lewis A., *Phys. Rev. D* **71**, 083008 (2005).
[34] K.M. Smith, W. Hu and M. Kaplinghat, *Phys. Rev. D* **70**, 043002 (2004).
[35] M. Kaplinghat, L. Knox and Y. Song, *Phys. Rev. Lett.* **91**, 241301 (2003).
[36] V. Acquaviva, C. Baccigalupi and F. Perrotta, *Phys. Rev. D* **70**, 023515 (2004).
[37] J. Hwang, *Astrophys. J.* **375**, 443 (1991).
[38] G. Esposito-Farese and D. Polarski, *Phys. Rev. D* **63**, 063504 (2001).
[39] F. Perrotta, C. Baccigalupi and S. Matarrese, *Phys. Rev. D* **61**, 023507 (2000).
[40] C. Schimd, J.-P. Uzan, A. Riazuelo, *Phys. Rev. D* **71**, 083512
[41] U. Seljak and M. Zaldarriaga, *Astrophys. J.* **469**, 437 (1996).
[42] C. Baccigalupi, S. Matarrese and F. Perrotta, *Phys. Rev. D* **62**, 123510 (2000).
[43] C. Baccigalupi and F. Perrotta, *Phys. Rev. D* **59**, 123508 (1999).
[44] M. Chevallier and D. Polarski, Int. J. Mod. Phys. D **10**, 213 (2001).
[45] E.V. Linder, *Phys. Rev. Lett.* **90**, 091301 (2003).
[46] C.P. Ma, R.R. Caldwell, P.Bode and L. Wang, *Astrophys. J. Lett.* **521**, L1 (1999).
[47] H. Kodama and M. Sasaki, Prog. Theor. Phys. Suppl. 78, 1 (1984).
[48] A.R. Liddle, R.J. Scherrer, *Phys. Rev. D* **59**, 023509 (1999).
[49] P.J. Steinhardt, L. Wang, I. Zlatev, *Phys. Rev. D* **59**, 123504 (1999).
[50] M. Bartelmann, F. Perrotta, C. Baccigalupi, *Astron. & Astrophys.* **396**, 21 (2002).
[51] B. Gold, *Phys. Rev. D* **71**, 063522 (2005)
[52] M. Zaldarriaga and U. Seljak, *Phys. Rev. D* **55**, 1830 (1997).
[53] K.M. Smith, W. Hu, M. Kaplinghat, astro-ph/0607315 (2006)
[54] A. Balbi, C. Baccigalupi, S. Matarrese, F. Perrotta, N. Vittorio, *Astrophys. J. Lett.* **588**, L5 (2003)
[55] W. Hu, D. Huterer, K.M. Smith, astro-ph/0607316 (2006)
[56] P. Oxley et al. 2004, Earth Observing Sustem IX. Edited by William L. Barnes and James J. Butler, Proceedings of the SPIE, 5543, 320